

Scheduled to appear in the ApJ 20 July 2006, v646n 1 issue

Sensitivity of time-distance helioseismic measurements to spatial variation of oscillation amplitudes I. Observations and a numerical model

S.P. Rajaguru¹, A.C. Birch², T.L. Duvall Jr.³, M.J. Thompson⁴, and J. Zhao¹

ABSTRACT

It is well known that the observed amplitude of solar oscillations is lower in sunspots than in quiet regions of the Sun. We show that this local reduction in oscillation amplitudes combined with the phase-speed filtering procedure in time-distance helioseismic analyses could be a source of systematic errors in the range of 5 - 40% in the measured travel-time anomalies of acoustic waves around sunspots. Removing these travel time artifacts is important for correctly inferring the subsurface structure of sunspots. We suggest an empirical correction procedure and illustrate its usage for a small sunspot. This work utilizes data from MDI/*SOHO*.

Subject headings: Sun: helioseismology — Sun: magnetic fields — Sun: oscillations — sunspots

1. Introduction

The stochastic nature of oscillation excitation due to turbulent convection is one major source of noise (i.e. realisation noise) and systematics in helioseismology (Christensen-Dalsgaard 2002). Another source of systematics is spatial modulation of the waves by active

¹W.W. Hansen Experimental Physics Laboratory, Stanford University, Stanford CA 94305, USA;
rajaguru@sun.stanford.edu

²Colorado Research Associates, NorthWest Research Associates, Inc., 3380 Mitchell Lane, Boulder, CO 80301.

³Laboratory for Solar and Space Physics, NASA Goddard Space Flight Center, Greenbelt, MD 20771.

⁴Department of Applied Mathematics, Hicks Building, University of Sheffield, Sheffield S3 7RH, UK.

regions and large-scale convection. Accounting for and reducing such noise and systematics is important in helioseismology, global (Woodard 1984; Duvall & Harvey 1986; Schou 1992; Libbrecht 1992) as well as local (Gizon and Birch 2004). Global helioseismic power spectral analyses use long uninterrupted observations towards this end (Libbrecht 1992; Christensen-Dalsgaard 2002). In contrast, determining localized non-axisymmetric perturbations inside the Sun – the main goal of local helioseismic techniques – necessarily involves using observations of more limited extent in both space and time. Such a task may appear more difficult and susceptible to larger uncertainties and systematics. The last two decades have witnessed the development and refinement of a new class of local techniques, that include helioseismic holography (Lindsey & Braun 1997), far-side imaging (Lindsey & Braun 2000) and time-distance helioseismology (Duvall et al. 1993), which have been fairly successful in achieving such tasks. These new techniques are based on studying quantifiable properties of causal connections that acoustic waves establish between points on the solar surface during their travel inside the Sun. These techniques are being fine-tuned, achieving increased sensitivity to local changes in the structure and dynamics of the Sun, e.g. sunspots (Kosovichev et al. 2000; Birch et al. 2004; Couvidat et al. 2004; Hughes et al. 2005; Lindsey & Braun 2005). At the same time, the necessity to accurately estimate the errors and systematics in the measurements is also being increasingly felt (Braun et al. 2004; Werne et al. 2004; Gizon and Birch 2004).

Time-distance helioseismology uses temporal cross-correlations of the oscillation signals from separated points on the solar surface (Duvall et al. 1993). The wave packet-like structure of such temporal cross-correlation signals is understood to be due to the propagation of wave packets formed by acoustic waves. The waves constituting a single wave packet travel with approximately the same horizontal phase speed and in the high frequency limit follow the same path inside the Sun (Duvall et al. 1993, 1997). Connection between the time-distance and modal frequency-wavenumber analyses have been studied by Kosovichev & Duvall (1997) and Bogdan (1997). Kosovichev & Duvall provided an useful formula to fit the time-distance correlation signals. Bogdan showed, with an explicit calculation, that a group of acoustic waves with approximately the same horizontal phase-velocity indeed interfere constructively to form a wave packet thereby leading to the observed structure of temporal cross-correlation signals. This understanding led to further refinement of time-distance measurement procedures (Duvall et al. 1997) that include phase-speed filtering: three-dimensional Fourier spectra of data cubes are filtered to select waves that travel with approximately the same horizontal phase speed and inverted back to the time domain to perform the cross-correlations. Such phase-speed filtering not only improves the signal-to-noise in travel time measurements, but also makes possible measuring travel times at very short travel distances (shallow depths and hence of the high degree modes). These

improvements are crucial in measuring travel times at each location keeping the original spatial resolution of the data, thereby allowing tomographic study of localized structures such as sunspots (e.g. Kosovichev & Duvall 1999; Kosovichev et al. 2000; Zhao et al. 2001).

In this paper we report on the identification of a significant source of systematics in travel-time measurements that arises due to an adverse coupling of localized strong spatial modulation of oscillation amplitudes in sunspots with the phase-speed filtering procedure. Further, we present a numerical model that describes this source of systematics.

2. Oscillation amplitudes and travel times

Largely reduced p-mode acoustic power observed in sunspots is thought to have contributions from several causes (Hindman et al. 1997) that are of two major physical origins: (i) the interaction between sunspot magnetic field and the quiet-sun p modes and convection, and (ii) radiative transfer effects induced by altered thermal conditions within the sunspot. The former physical process is thought to be responsible for (a) absorption of p modes as known from a number of studies following the work of Braun et al. (1988), (b) alteration of the p-mode eigenfunctions (Jain et al. 1996; Hindman et al. 1997), and (c) reduced excitation of p modes within the sunspot. The latter radiative transfer effects cause (a) changes in the formation height of spectral lines used to measure the velocities within spots (Balthasar & Schmidt 1993; Bogdan 2000), and (b) imperfect measurements through changes in the spectral line profile due to Zeeman splitting and the darkness of the spot (Alamanni et al. 1990; Wachter et al. 2006). The spatial variation of acoustic power can be determined from Doppler images by forming pixel-wise temporal power spectra and summing the power in the p-mode band of frequencies (Hindman & Brown 1998; Thomas & Stanchfield 2000; Nicholas et al. 2004). Here, we calculate p-mode power within a band of frequencies between 1.7 and 5.3 mHz over three active regions containing a small, medium and large sized spots using MDI Doppler velocity data (high-resolution data for the small and medium size spots, and full-disk resolution data for the large spot) (Scherrer et al. 1995). The NOAA AR numbers for these three sunspots are respectively, AR8555, AR8243 and AR10488. We find that quiet-sun regions devoid of any significant magnetic field show p mode power that is more or less homogeneous over the solar surface. When a sufficient number of individual pixel values (or realizations) are averaged over, the p mode power is nearly a constant over space in the quiet-sun (Venkatakrishnan et al. 2001). To determine the relative deviations that active regions introduce in the p mode power we normalize the power distribution within an active region with respect to a quiet-sun spatial average. The quiet-sun regions chosen for the normalization are from within the larger regions covering the sunspots and are of the

same latitudinal extent as the active regions but are outside of any significant magnetic field. We call the square root of such a spatial power map the oscillation ‘amplitude modulation function’, $A(\mathbf{x})$, where \mathbf{x} is the horizontal position on the solar surface. Note that $A(\mathbf{x})$ is derived by averaging over the p-mode band (1.7 – 5.3 mHz), but, in general, amplitude modulations are frequency dependent. Figure 1 displays $A(\mathbf{x})$ derived for the three active regions chosen, with their MDI magnetograms shown as well. We note here that detailed studies of local magnetic modulations of oscillation power and their relation to the local magnetic field strengths have been reported by Hindman & Brown (1998) and Nicholas et al. (2004). The latter authors have also constructed simple models which allow a comparison with the changes in modal power distribution determined from ring diagram (normal mode) analyses (Rajaguru et al. 2001).

The measured spectrum of oscillations in the presence of such long lived spatial modulation of oscillation amplitudes is the convolution, in wavenumber space, of the frequency-wavenumber spectrum of oscillations with the wavenumber spectrum of the modulating function. The possible errors that such convolutions would introduce in the modal parameters could be reduced by using an observational time series sufficiently longer than the life span of amplitude modulators. Such a way of reducing the systematics is not available in local helioseismology, where the objective is to probe perturbations localized in space and time. However, a purely *time-space analysis* of the oscillation field, in contrast to a *frequency-wavenumber analysis*, would not be subject to the kind of errors from which a modal power-spectral analysis suffers. For example, in time-distance analysis, a temporal cross-correlation of oscillation signals from two locations is not affected by a stationary scaling of oscillation amplitudes and hence the (phase) travel times are not affected. However, the intermediate step of phase-speed filtering, with recourse to Fourier space to select waves of certain modal relations as explained in the previous section, couples the scales or wavenumbers of the modulating function to the oscillation spectra. This causes perturbations in the wavenumbers of the oscillation spectra which in turn manifests as perturbations in travel times measured over regions where the oscillation amplitudes are modulated.

Before examining this effect by way of a numerical model of the measurement procedures in the next section, we first demonstrate the changes in travel times as measured using a standard time-distance analysis procedure using MDI velocity data cubes. We perform experiments using artificial amplitude modulation functions $A_a(\mathbf{x})$, which bring out the essential features of the coupling between the spatial variation of oscillation amplitudes and the frequency-wavenumber spectrum of the phase-speed filter. We choose two forms for $A_a(\mathbf{x})$ for this purpose; horizontal one-dimensional cuts across these modulation functions are shown in the top row of Figure 2a. We have chosen a peak suppression of 80% (which is typical of umbrae of medium sized spots, see Figure 1) for both functions. The Gaussian form, denoted

as $A_{a,g}$ (top left panel in Figure 2a), has a FWHM of about 16 Mm while the disc-like function, denoted as $A_{a,d}$ (top right panel in Figure 2a), has a sharp spatial gradient connecting zero suppression to the peak suppression, which is spread over a disc of diameter 16 Mm. Each velocity image of a very quiet region data cube is multiplied by $A_a(\mathbf{x})$ before running the data through a standard time-distance analysis procedure that includes phase-speed filtering and uses center-annulus geometry for computing cross-correlations (Duvall et al. 1997; Rajaguru et al. 2004). Travel time maps are calculated for the range in travel distances Δ that are normally used in tomographic inversions (Kosovichev & Duvall 1999; Couvidat et al. 2004; Hughes et al. 2005), and are compared with those obtained for the original quiet-sun data (without introducing any amplitude variations). The shifts in mean phase travel times, i.e. mean of ingoing and outgoing wave phase travel times, $\delta\tau_{\text{mean}} = \tau_{\text{mean}}(\text{masked}) - \tau_{\text{mean}}(\text{quiet})$, as a function of Δ are shown as maps in Figure 2. Hereafter, by travel times we always refer to mean phase travel times and remove the subscript 'mean' in the notations, i.e. $\delta\tau = \delta\tau_{\text{mean}}$. Figure 3 shows these $\delta\tau$ spatially averaged over the masked area, which is about 16 Mm in diameter, and denoted as $\delta\tau_{\text{av}}$, as a function of Δ . The results in Figure 2 and 3a show the following main features of amplitude suppression on travel times. Firstly, steeper spatial gradients in the amplitude suppression cause larger shifts in travel times (compare left and right columns in Figure 2) in addition to the proportional changes caused by the amount of suppression. Secondly, smaller Δ show positive shifts in travel times (longer travel times), while the larger Δ show the opposite change (shorter travel times), with the change over occurring at larger Δ for larger spatial gradient suppression. Thirdly, the magnitude of $\delta\tau_{\text{av}}$ decreases as Δ increases.

To estimate changes in travel times that sunspots could introduce purely due to the spatial variation that they cause in the oscillation amplitudes, we then apply $A(\mathbf{x})$ determined from the pixel-wise power map as explained earlier and shown in Figure 1 to the same quiet-sun patch data cube and compare the travel-time maps obtained with and without the application of $A(\mathbf{x})$. The results for $\delta\tau$ are shown in Figure 4, similarly to that shown in Figure 2. Figure 3b compares the Δ dependence of $\delta\tau_{\text{av}}$, which are averaged $\delta\tau$ over the surface area of the spots, for the small, medium and large sized spots.

How do the changes we have measured and shown in Figures 2 – 4, which are purely due to the combined action of spatial amplitude variation and phase-speed filtering, compare with the actual travel times measured in sunspot regions? For this purpose, we have measured the mean travel-time shifts over the three sunspot regions shown in Figure 1 with exactly the same measurement procedure as for the results shown in Figures 2 – 4. The Δ dependence of $\delta\tau = \tau(\text{spot}) - \tau(\text{quiet})$ averaged over the area of the spots is shown in Figure 5a. The fractional values, with respect to the $\delta\tau_{\text{av}}$ measured for these spots, of the similar changes measured over the amplitude modulated areas shown in Figure 3 are shown in panels b)

and c) of Figure 5. In summary, the results in Figures 2 – 5 show that spatially localized amplitude variations in the oscillation field caused by sunspots (Fig. 1), in combination with the phase-speed filtering in the analysis procedure, can account for mean travel-time shifts in the range of 5 – 40% in the observed travel-time anomalies in sunspots.

A simple experiment of applying the amplitude modulation after the phase-speed filtering leads to negligible changes in travel time. This proved to us that the effect was caused by the interaction of the phase-speed filter with the amplitude modulation. A clear understanding of the origin, and a method of accounting for it in the travel times measured in sunspots, of such changes are important because these can be a source of systematic errors in the subsurface inferences derived using differential inversion methods such as are described in Gizon and Birch (2005) and references therein. In the next section we build a numerical model of the action of phase-speed filter and its interaction with an amplitude function $A(\mathbf{x})$.

3. Action of a Phase-Speed filter

In this section we derive a simple model showing the effect of the amplitude suppression function $A(\mathbf{x})$ on the center-to-annulus cross-covariance and hence the center-to-annulus travel time. The three generic steps in computing center-to-annulus cross-covariances are to filter the data, average the data over the annulus and over a small region around the center point to obtain the “annulus” and “center” signals, and then to compute the cross-covariance of the “center” and “annulus” signals (Duvall et al. 1997). We write the observed oscillation signal, ϕ , e.g. the line-of-sight component of the velocity at the solar surface as,

$$\phi(\mathbf{x}, t) = A(\mathbf{x})\psi(\mathbf{x}, t), \quad (1)$$

where $\psi(\mathbf{x}, t)$ is the underlying oscillation signal, i.e. the signal that would be seen if the sunspot had no effect on the oscillation amplitude. Horizontal position is given by \mathbf{x} and time by t .

The first step is to filter the observed signal. This is performed in the Fourier domain (\mathbf{k}, ω) by multiplying the Fourier transform of the observed signal, $\phi(\mathbf{k}, \omega)$, by a filter function $\mathcal{F}(\mathbf{k}, \omega)$:

$$\phi_f(\mathbf{k}, \omega) = \mathcal{F}(\mathbf{k}, \omega)\phi(\mathbf{k}, \omega) \quad (2)$$

This filtering can be transformed back from wavenumber to the space domain as a convolution over space:

$$\phi_f(\mathbf{x}, \omega) = \mathcal{F}(\mathbf{x}, \omega) \otimes \phi(\mathbf{x}, \omega) \quad (3)$$

where $\mathcal{F}(\mathbf{x}, \omega)$ is the inverse Fourier transform over wavenumber \mathbf{k} of the filter function $\mathcal{F}(\mathbf{k}, \omega)$ and \otimes is a convolution over space \mathbf{x} . Using the convention for discrete Fourier

transforms given in Appendix 1 of Gizon & Birch (2004), Eq. 3 can be rewritten as,

$$\phi_f(\mathbf{x}, \omega) = \frac{h_x^2}{(2\pi)^2} \sum_{\mathbf{x}'} \mathcal{F}(\mathbf{x} - \mathbf{x}', \omega) \phi(\mathbf{x}', \omega), \quad (4)$$

where the sum over surface position \mathbf{x}' is taken over all points where $\mathcal{F}(\mathbf{x} - \mathbf{x}', \omega)$ is not zero, and h_x is the grid spacing in the horizontal directions (near disk center $h_x = 1.39$ Mm for full-disk MDI data and $h_x = 0.83$ Mm for two-by-two binned high-resolution MDI data).

The second step is to average the filtered signal over the annulus and then, separately, over a small region around the center point to obtain the “annulus” and “center” signals respectively (see Rajaguru et al. (2004) for a detailed description of the exact procedure employed in this paper) In general we can write

$$\phi_{\text{annulus}}(\mathbf{x}, \Delta, \omega) = \sum_{\mathbf{x}'} f_{\text{annulus}}(\mathbf{x}' - \mathbf{x}, \Delta) \phi_f(\mathbf{x}', \omega), \quad (5)$$

$$\phi_{\text{center}}(\mathbf{x}, \omega) = \sum_{\mathbf{x}'} f_{\text{center}}(\mathbf{x}' - \mathbf{x}) \phi_f(\mathbf{x}', \omega), \quad (6)$$

where $f_{\text{annulus}}(\mathbf{x}, \Delta)$ and $f_{\text{center}}(\mathbf{x})$ are the weight functions for obtaining the “annulus” and “center” signals from the filtered data (Rajaguru et al. 2004). Combining the above equations (Eqs. [5-6]) with equation (4) we obtain

$$\phi_{\text{annulus}}(\mathbf{x}, \Delta, \omega) = \sum_{\mathbf{x}'} W_{\text{annulus}}(\mathbf{x}' - \mathbf{x}, \Delta) \phi(\mathbf{x}', \omega), \quad (7)$$

$$\phi_{\text{center}}(\mathbf{x}, \omega) = \sum_{\mathbf{x}'} W_{\text{center}}(\mathbf{x}' - \mathbf{x}) \phi(\mathbf{x}', \omega), \quad (8)$$

with the weight functions W given by

$$W_{\text{annulus}}(\mathbf{x}, \Delta, \omega) = \frac{h_x^2}{(2\pi)^2} \sum_{\mathbf{x}'} f_{\text{annulus}}(\mathbf{x}' + \mathbf{x}, \Delta) \mathcal{F}(\mathbf{x}', \omega) \quad (9)$$

$$W_{\text{center}}(\mathbf{x}, \Delta, \omega) = \frac{h_x^2}{(2\pi)^2} \sum_{\mathbf{x}'} f_{\text{center}}(\mathbf{x}' + \mathbf{x}) \mathcal{F}(\mathbf{x}', \omega). \quad (10)$$

We have now expressed (Eqs. [7]-[8]) the “center” and “annulus” signals as averages of the unfiltered data. The weight functions W_{annulus} and W_{center} express the weights with which the raw data are averaged, at each temporal frequency, to obtain these average signals. Figure 6 shows an example of these weight functions. In general, the weight functions are not well localized as a result of the strong horizontal wavenumber dependence of the phase-speed filtering.

The final step is to compute the cross-covariance of the “center” and “annulus” signals. This cross-covariance, for center position \mathbf{x} and annulus with radius Δ , is given by

$$C(\mathbf{x}, \Delta, \omega) = 2\pi\phi_{\text{center}}^*(\mathbf{x}, \omega)\phi_{\text{annulus}}(\mathbf{x}, \Delta, \omega). \quad (11)$$

Employing equations (7) and (8) we can write equation (11) as

$$C(\mathbf{x}, \Delta, \omega) = \sum_{\mathbf{x}', \mathbf{x}''} W_{\text{center}}^*(\mathbf{x}' - \mathbf{x})W_{\text{annulus}}(\mathbf{x}'' - \mathbf{x})C^\phi(\mathbf{x}', \mathbf{x}'', \omega) \quad (12)$$

where the point-to-point cross-covariance of ϕ is

$$C^\phi(\mathbf{x}', \mathbf{x}'', \omega) = 2\pi\phi^*(\mathbf{x}', \omega)\phi(\mathbf{x}'', \omega). \quad (13)$$

We can express equation (12) in terms of the covariance of the underlying wavefield ψ by noticing that the point-to-point cross-covariance of ϕ can be written in terms of the point-to-point cross-covariance, C^ψ , of the underlying wavefield, ψ , and the amplitude suppression function A as

$$C^\phi(\mathbf{x}', \mathbf{x}'', \omega) = 2\pi A(\mathbf{x}')A(\mathbf{x}'')\psi^*(\mathbf{x}', \omega)\psi(\mathbf{x}'', \omega). \quad (14)$$

As a result, the center-to-annulus cross-covariance of ϕ is

$$C(\mathbf{x}, \Delta, \omega) = \sum_{\mathbf{x}', \mathbf{x}''} W_{\text{center}}^*(\mathbf{x}' - \mathbf{x})W_{\text{annulus}}(\mathbf{x}'' - \mathbf{x})A(\mathbf{x}')A(\mathbf{x}'')C^\psi(\mathbf{x}', \mathbf{x}'', \omega). \quad (15)$$

This is the desired result; we have the center-to-annulus cross-covariance of the filtered wavefield in terms of the point-to-point cross-covariance of the underlying wavefield ψ . As described in Gizon & Birch (2004) we can compute C^ψ in terms of only the power spectrum of ψ . The weight functions W depend only on the filter function and the averaging done to obtain the “center” and “annulus” signals. Thus, for a given measurement scheme (i.e. filter and spatial averaging scheme) and for a particular power spectrum of the underlying wavefield, we can compute how the center-to-annulus cross-correlation of the modified wavefield depends on the amplitude function A . From equation (15) we can see that the effect of an amplitude function is to alter the weights with which different two-point cross-covariances contribute to the full center-to-annulus cross-covariance.

In order to demonstrate the validity of equation (15) we computed the cross-covariances $C(\mathbf{x}, \Delta, \omega)$ for the case shown in the top left panel of Figure 4: this case corresponds to applying the amplitude variation measured over the small sunspot (spot 1) to a quiet-sun patch and measuring the travel-time shifts for a distance Δ of 4.96 Mm.

In Figure 7 we show a comparison of the travel times shown in Figure 4 (top left panel) with the travel times measured from $C(\mathbf{x}, \Delta, \omega)$ predicted by equation (15). We see that the model presented in this section predicts the effect of the amplitude function A reasonably well.

4. An empirical correction procedure

The results in the previous two sections show that systematic shifts in travel times are caused by the interaction of the spatial variation in oscillation amplitudes, be they of any origin (as demonstrated by our experiments with artificial modulation functions), with the phase-speed filtering in the analysis procedure. This understanding shows that if we could remove the strong spatial variation in the oscillation amplitudes, caused by the objects of our main concern, i.e. sunspots, without affecting the temporal phase evolution of oscillation signals, then this particular effect could be reversed thereby removing the systematic shifts. This suggests that the oscillation signal at each pixel could be boosted up by a constant factor obtained from the amplitude function $A(\mathbf{x})$ (Fig. 1) derived from the pixel-wise power maps: a simple way of estimating the pixel-wise scale-up factor is just taking the inverse of $A(\mathbf{x})$.

A natural way to carry out this remedy is to boost the amplitude of the oscillation signal in each pixel over the sunspot region so that the functions $A(\mathbf{x})$ look smoother and have values similar to that of the more or less homogeneous quiet-sun regions. We choose the case of the small sunspot (spot 1) shown in the top row of Figure 1. The pixel-wise scale-up factor is given by $S_f(\mathbf{x}) = 1/A(\mathbf{x})$. Here, we concern ourselves with correcting the power deficit only within the sunspot, and so we determine the scale-up factor S_f in a small area in and around the sunspot. The sunspot (spot 1) is found to be about 14 Mm in diameter, as seen in $A(\mathbf{x})$ (top left panel in Figure 1), and we choose an area of about 28 Mm square centered around this spot and calculate $S_f(\mathbf{x})$ in this region. To minimize the effects of pixel-scale variations we smooth S_f by a four pixel box car. The resulting map of the scale-up factor is shown in Figure 8a. We note that $A(\mathbf{x})$ was determined for p modes within a frequency band of 1.7 – 5.3 mHz. Hence we use S_f calculated as above to boost the amplitudes of p modes in the same band of frequencies, i.e. we apply S_f in Fourier space to boost the amplitudes of p modes in this band. These are then inverted back to the time-space domain to get the corrected Doppler velocity data cube that is subjected to the same time-distance analysis procedure as before (Section 2). Figure 8b shows the frequency distribution of power averaged over the sunspot pixels (an area of 14 Mm square around the spot center) before and after correction, i.e. before and after applying S_f , and also quiet-sun power averaged over an area of the same size. We note here that such artificial enhancement of oscillation amplitudes will not undo the real physical changes in travel times that the spots have caused, but are expected to undo the changes arising from the amplitude modulations demonstrated in the previous section.

We calculated maps of changes in mean phase travel times, $\delta\tau = \delta\tau(\text{spot}) - \delta\tau(\text{quiet})$, before and after the amplitude or power corrections described above. The results for two representative travel distances Δ of 4.96 and 16.5 Mm are shown in the two columns of Figure

9. The top row shows the original or uncorrected travel times $\delta\tau_o$, the middle row shows the corrected travel times $\delta\tau_c$, and in the bottom row are shown the differences $\delta\tau_o - \delta\tau_c$. It is instructive to compare $\delta\tau_o - \delta\tau_c$ with the corresponding panels (i.e. for the same Δ) in Figures 2 and 4: the corrections $\delta\tau_o - \delta\tau_c$ are of the same sign and of similar magnitude as that of $\delta\tau$ in Figures 2 and 4. This suggests that the simple amplitude-boosting correction scheme presented here reduces, to some extent, the systematic shift in the travel times caused by the reduction of oscillation amplitudes in the sunspot. Possible complications for the correction scheme include the spatial averaging that was used to create the scale-up function S_f , noise in the estimate of the amplitude suppression function $A(\mathbf{x})$, and frequency dependence of the real solar suppression of oscillation amplitudes. A more detailed analysis of this correction scheme and also some variants of it, including a study of how the corrections in travel times affect the subsurface inferences through inversions, is left for a separate paper (Paper II) (Zhao et al. 2006).

5. Discussion

The change in travel times in response to changes in surface oscillation amplitudes depends on the spatial gradient of the amplitude modulation, the amount of reduction in the amplitudes, the travel distances, and the details of the phase-speed filter. The principal finding is that the largest and significant changes occur only for waves with short travel distances (Δ up to about 16 Mm). Values in the range of 5 - 40% of the travel-time anomalies that sunspots cause could be a result of oscillation amplitude reduction (Figure 5b). This might indicate that the subsurface inferences from inversions would, correspondingly, undergo significant changes for the near-surface layers. However, the exact amount of changes and how the particular Δ dependence of $\delta\tau$ that we have shown here would influence the inferences regarding deeper layers can only be assessed by doing detailed analyses of inversions. We have shown that a simple correction, which involves boosting up the p-mode amplitudes, is able to reverse the interaction of amplitude suppression and phase-speed filtering thereby removing substantially the systematic changes or artifacts in travel times. We have shown this for the case of a small sunspot, where there is a measurable amount of p-mode power within the umbra. In large and very dark sunspots, the signal-to-noise ratio for the p-mode signal in the umbrae is too low to carry out this correction successfully.

We have demonstrated that the effects of oscillation amplitude variations on travel times are caused by the phase-speed filtering procedure, which is however crucial to achieving high signal-to-noise as well as high spatial resolution in the measurements of travel times. Spatial amplitude modulations (convolutions in Fourier space) and the phase-speed filtering

are non-commuting operations in the frequency-wavenumber (Fourier) domain. The travel distance Δ dependence of the systematic changes in travel times $\delta\tau$ are seen to be of the same form as the actual travel-time anomalies measured over sunspots (compare Figures 3b and 5a). In spite of such a similarity between the systematic errors and the real changes in $\delta\tau$ for sunspots, it is important that the other known signatures that sunspots leave in local helioseismic measurements are differentiated from the above. In particular, sunspots show large asymmetries measured in both the amplitudes of cross-covariances and travel times (Duvall et al. 1996), as well as in the control-correlation ingression and egression measurements of helioseismic holography (Lindsey & Braun 2005), between the out- and in-going wave correlations. These asymmetries possibly relate to the irreversible changes in acoustic waves impinging on real sunspots and hence their origin is independent of the travel-time shifts that we have shown here. The contributions due to the effect that we have studied here are also likely to be present in the helioseismic holography studies (Lindsey & Braun 1997, 2005); because these studies do involve selecting in Fourier space modes of certain frequency-wavenumber range, and hence a similar influence as that of a phase-speed filter is possible.

This work utilizes data from the Solar Oscillations Investigation/ Michelson Doppler Imager (SOI/MDI) on the Solar and Heliospheric Observatory (SOHO). The MDI project is supported by NASA grant NAG5-13261 to Stanford University. SOHO is a project of international cooperation between ESA and NASA. The work in part was supported by the UK Particle Physics and Astronomy Research Council (PPARC) through grants PPA/G/S/2000/00502, PPA/V/S/2000/00512 and PP/X501812/1. The work of ACB was supported by NASA contract NNH04CC05C. SPR thanks Dr. A.G. Kosovichev for discussions and critical comments. We thank Dr. Douglas Braun for useful comments.

REFERENCES

- Alamanni, N., Cavallini, F., Ceppatelli, G. & Righini, A. 1990, *A&A*, 228, 517
- Balthasar, H., & Schmidt, W. 1993, *A&A*, 279, 243
- Birch, A.C., Kosovichev, A. G., & Duvall, T. L., Jr. 2004, *ApJ*, 608, 580
- Bogdan, T.J. 1997, *ApJ*, 477, 475
- Bogdan, T.J. 2000, *Sol. Phys.*, 192, 373
- Bogdan, T. J., Hindman, B. W., Cally, P. S., Charbonneau, P. 1996, *ApJ*, 465, 406

- Braun, D. C., La Bonte, B. J., & Duvall, T. L., Jr. 1987, *ApJ*, 319, L27
- Braun, D. C., La Bonte, B. J., & Duvall, T. L., Jr. 1988, *ApJ*, 335, 1015
- Braun, D.C., & Lindsey, C. 1999, *ApJ*, 513, L79
- Braun, D.C., Lindsey, C. ,& Birch, A.C. 2004, *BAAS*, 204, 530
- Christensen-Dalsgaard, J. 2002, *Rev. Mod. Phys.*, 74, 1073
- Couvidat, S., Birch, A.C., Kosovichev, A. G., & Zhao, J. 2004, *ApJ*, 607, 554
- Duvall, T. L., Jr., & Harvey, J. W. 1986, in *Seismology of the Sun and the Distant Stars*, ed. D.O. Gough (Dordrecht Reidel), 105
- Duvall, T. L., Jr., Jefferies, S. M., Harvey, J. W. & Pomerantz, M. A. 1993, *Nature*, 362, 430
- Duvall, T. L. Jr., D'Silva, S., Jefferies, S. M., Harvey, J. W., & Schou, J. 1996, *Nature*, 379, 235
- Duvall, T. L., Jr. et al. 1997, *Sol. Phys.*, 170, 63
- Gizon, L., & Birch, A.C. 2004, *ApJ*, 614, 472
- Gizon, L., & Birch, A.C. 2005, *Living Rev. Solar Phys.* 2, 6. URL (cited on 1/1/06): <http://www.livingreviews.org/lrsp-2005-6>
- Hindman, B.W., & Brown, T.M. 1998, *ApJ*, 504, 1029
- Hindman, B.W., Jain, R., & Zweibel, E.G. 1997, *ApJ*, 476, 392
- Hughes, S.J., Rajaguru, S.P., & Thompson, M.J. 2005, *ApJ*, 627, 1040
- Jain, R., Hindman, B.W., & Zweibel, E.G. 1996, *ApJ*, 464, 476
- Kosovichev, A.G., Duvall, T.L., Jr. in *SCORE-96: Solar Convection and Oscillations and Their Relationship*, ed. F.P. Pijpers et al., 1997 (Kluwer)
- Kosovichev, A.G., Duvall, T.L., Jr. 1999, *Current Science*, 77, 1467
- Kosovichev, A.G., Duvall, T.L., Jr., Scherrer, P.H. 2000, *Sol. Phys.*, 192, 159
- Libbrecht, K.G. 1992, *ApJ*, 387, 712
- Lindsey, C., & Braun, D.C. 1997, *ApJ*, 485, 895

- Lindsey, C., & Braun, D.C. 2000, *Science*, 287, 1799
- Lindsey, C., & Braun, D.C. 2005, *ApJ*, 620, L1107
- Nicholas, C.J., Thompson, M.J., & Rajaguru, S.P. 2004, *Sol. Phys.*, 225, 213
- Rajaguru, S.P., Basu, Sarbani, & Antia, H.M., 2001, *ApJ*, 563, 410
- Rajaguru, S.P., Hughes, S.J., & Thompson, M.J. 2004, *Sol. Phys.*, 220, 381
- Scherrer, P.H., et al. 1995, *Sol. Phys.*, 162, 219
- Schou, J. 1992, Ph.D. Thesis, Aarhus Univ., Denmark.
- Thomas, J.H. & Stanchfield II, D.C.H., 2000, *ApJ*, 537, 1086
- Venkatakrishnan, P., Kumar, Brajesh & Tripathy, S. C., 2001 *Sol. Phys.*, 202, 229
- Wachter, R. et al. 2006, in preparation
- Werne, J., Birch, A.C., & Julien, K. 2004, in *Proceedings of SOHO 14/GONG 2004 "Helio- and Asteroseismology: Towards a Golden Future"*, ed. Danesy, P. et al, p 172
- Woodard, M.F. 1984, Ph.D. Thesis, Univ. California, San Diego.
- Zhao, J., Kosovichev, A.G., & Duvall, T.L., Jr. 2001, *ApJ*, 557, 384
- Zhao, J. et al. 2006, in preparation (Paper II)

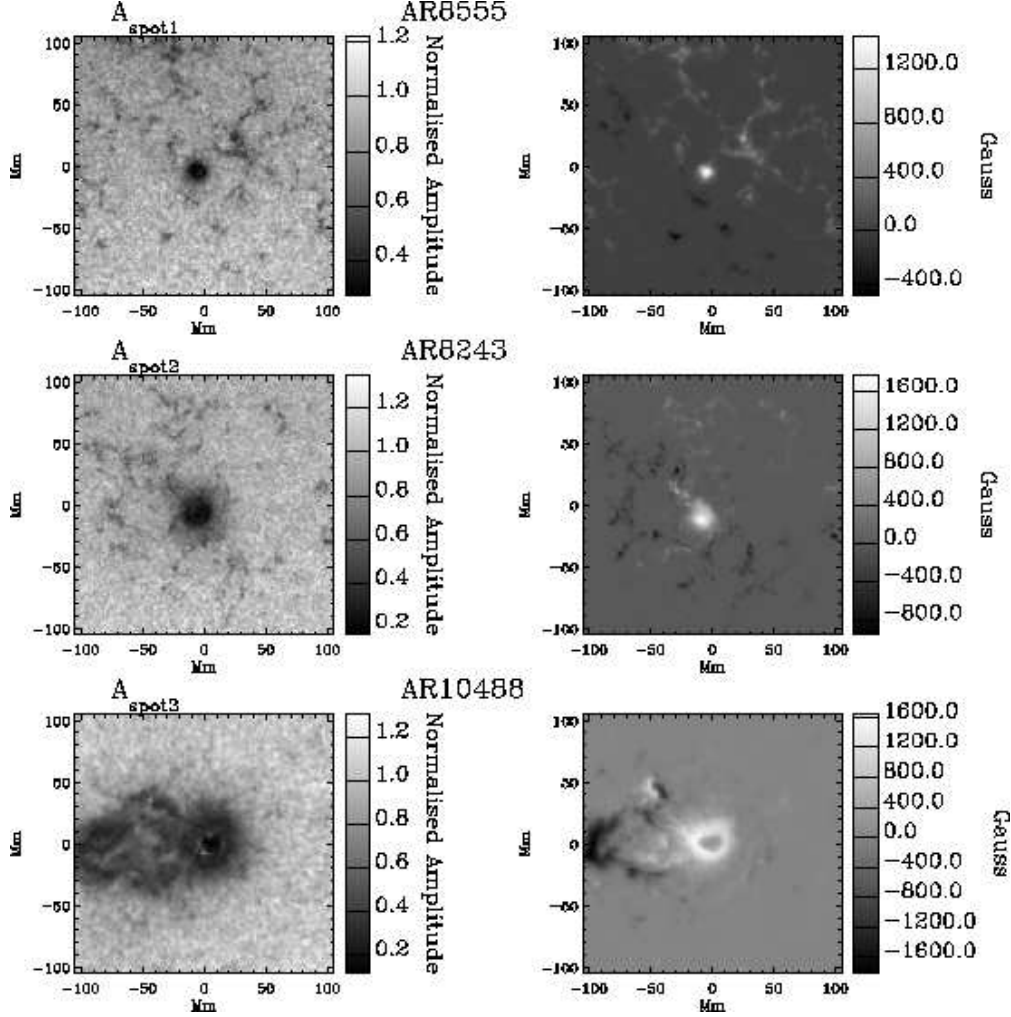


Fig. 1.— Spatial variation of oscillation amplitudes in the p-mode band, denoted as $A(\mathbf{x})$ and defined in the text, normalized to a quiet-sun spatial average, over small, medium and large sized sunspot regions as measured from a 512 minute MDI Doppler line of sight velocity data cubes. The small and medium sized spots' measurements are from high-resolution, and the large sized spot's is from full disk resolution MDI data. The right side panels show the corresponding time-averaged MDI magnetograms.

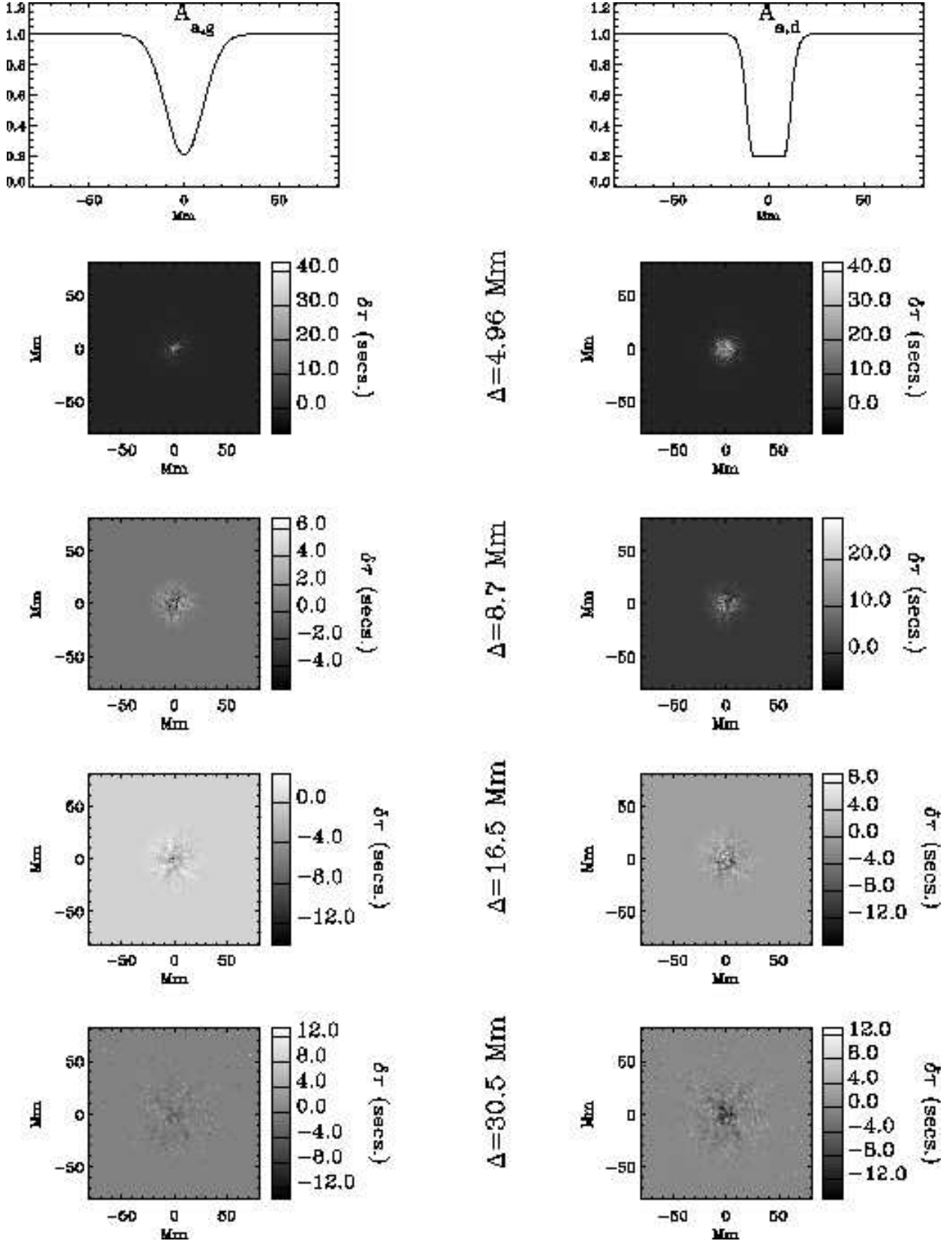


Fig. 2.— Changes in mean phase travel times, $\delta\tau$, introduced by oscillation amplitude modulation (spatial) functions $A_{a,g}(\mathbf{x})$: one dimensional cuts through the center of these azimuthally symmetric 2-d functions are shown in the top row, and $\delta\tau$ are shown below

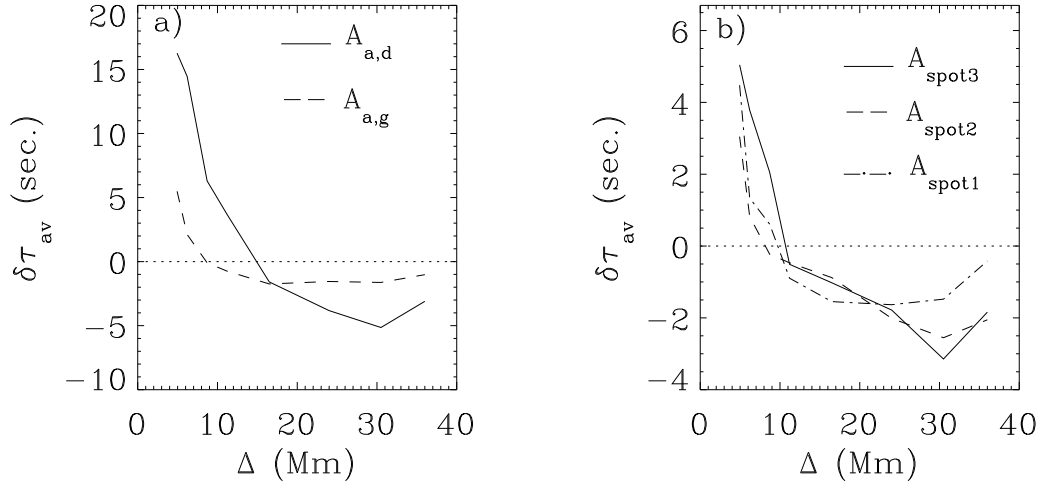


Fig. 3.— The changes in mean phase times spatially averaged over the masked area, $\delta\tau_{av}$, as a function of travel distance Δ . Panel *a*): for amplitude functions $A_{a,g}(\mathbf{x})$, and the spatial area averaged over is 16 Mm in diameter around the peak suppression. Panel *b*): for $A(\mathbf{x})$ derived from sunspot regions shown in Figure 1 and spatial averages are over the area of sunspots as seen in the magnetograms.

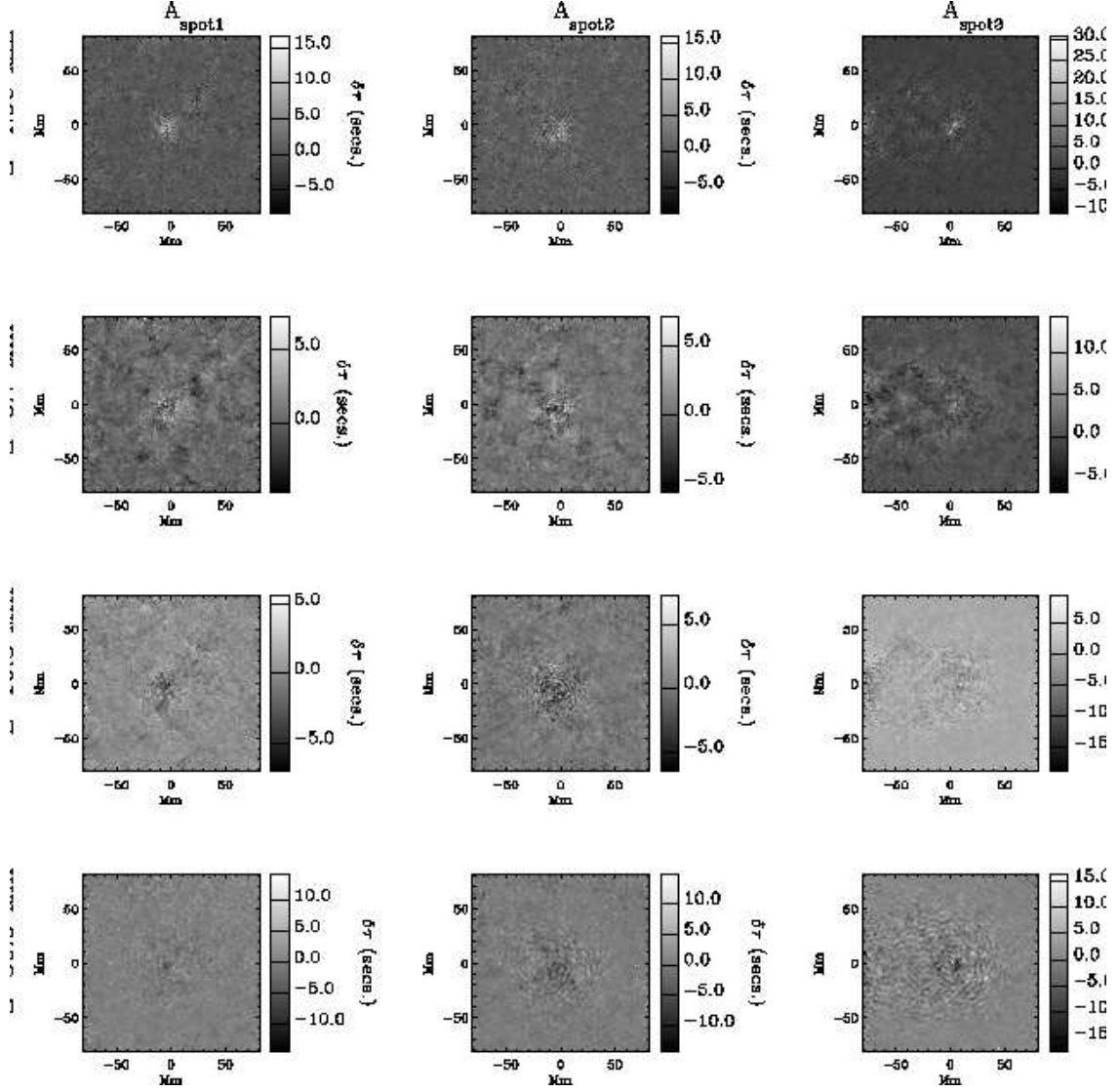


Fig. 4.— Same as in Figure 2 but for amplitude functions $A(\mathbf{x})$ derived from sunspot regions that are shown in Figure 1.

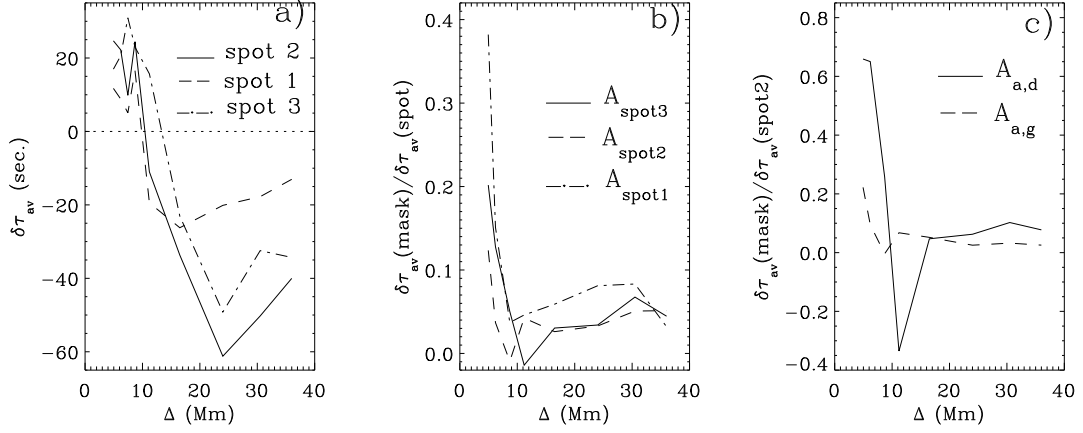


Fig. 5.— Panel a): spatial average of $\delta\tau = \tau(\text{spot}) - \tau(\text{quiet})$ measured over the three sunspots (Figure 1) as a function of Δ . Panel b): the fractional values of the average shifts, shown in Figure 3b, with respect to those shown in panel a) here for the three spots; and in panel c) are those in Figure 3a scaled by that of medium sized spot (spot 2).

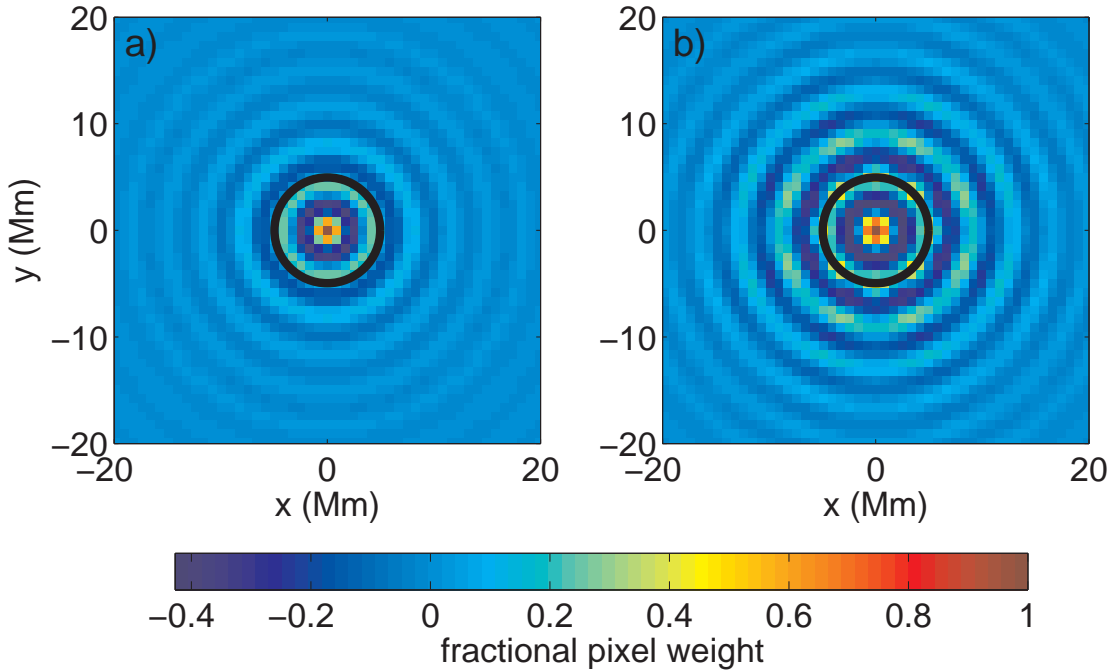


Fig. 6.— Spatial dependence of weight functions at fixed $\omega/2\pi = 3.9$ mHz and distance $\Delta = 4.96$ Mm. Panel a shows W_{center} and panel b shows W_{annulus} . In both cases the heavy black line shows the nominal distance, Δ .

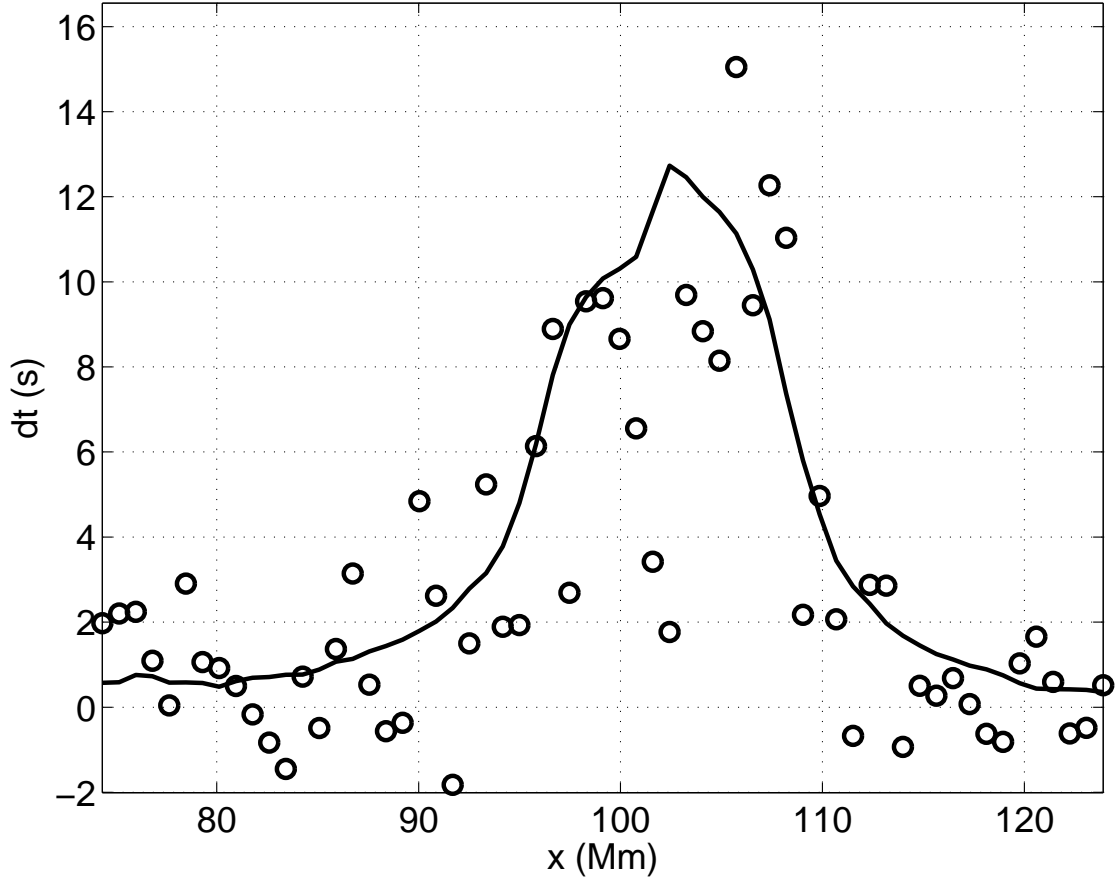


Fig. 7.— Travel time measured from the theoretical cross-covariances (Eq. [15]), solid line, and travel times measured from the masking experiment shown in Figure 4a (top left panel) at $y \approx 98$ Mm. There is good qualitative agreement within the noise level of the data.

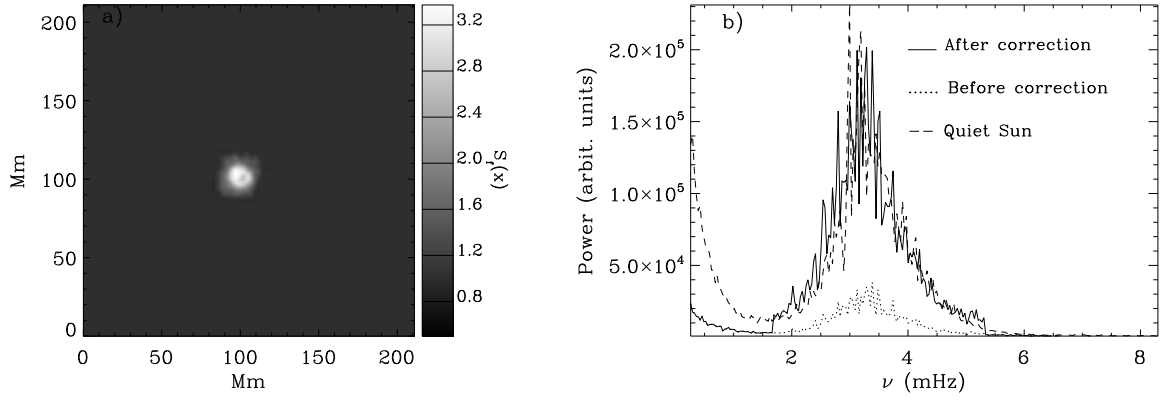


Fig. 8.— Panel *a*): spatial map of scale-up factor $S_f(\mathbf{x})$ determined around the sunspot of Figure 1 (top row). This is the factor by which p-mode amplitudes are boosted up. The frequency distribution of power averaged over sunspot pixels before (*dotted line*) and after (*solid line*) the corrections is shown in panel *b*); power averaged over a same number of quiet-sun pixels is shown as *dashed line*

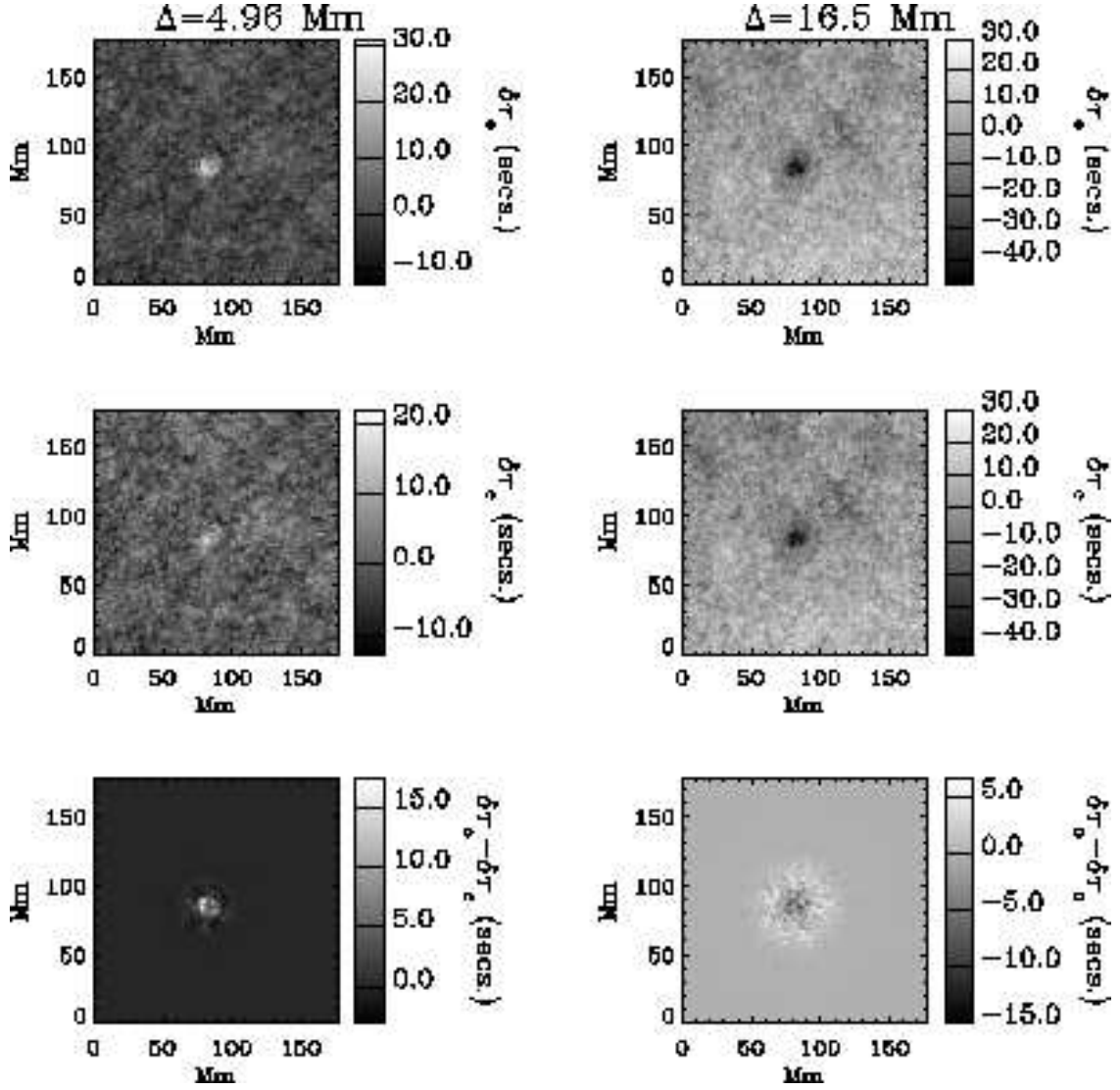


Fig. 9.— Maps of changes in mean phase travel times $\delta\tau$ over the small sunspot (spot 1) region for two Δ (in the two columns). In the top row are the original (uncorrected) travel times $\delta\tau_o$, in the middle row are the corrected ones $\delta\tau_c$, and the bottom row shows the corrections $\delta\tau_o - \delta\tau_c$.